

Squark-mediated Higgs+jets production at the LHC

J. Duarte*,¹ C. Peña,¹ A. Wang†,¹ M. Pierini,² and M. Spiropulu¹

¹*Caltech, 1200 E California Blvd, Pasadena, CA 91125 USA*

²*CERN, Rte de Meyrin, Geneve, 1211 Switzerland*

(Dated: September 19, 2018)

We investigate possible scenarios of light-squark production at the LHC as a new mechanism to produce Higgs bosons in association with jets. The study is motivated by the SUSY search for H+jets events, performed by the CMS collaboration on $\sqrt{s} = 8, 13$ TeV data using the *razor* variables. Two simplified models are proposed to interpret the observations in this search. The constraint from Run I and the implications for Run II and beyond are discussed.

PACS numbers:

INTRODUCTION

The ATLAS and CMS collaborations have searched intensively for SUSY production in the data collected at a center-of-mass energy $\sqrt{s} = 8$ TeV in 2012. A large part of the searches focused on SUSY models with conserved R-parity, for which the lightest SUSY particle (LSP) is stable. The LHC is particularly sensitive to the production of SUSY partners charged under QCD (squarks and gluinos), given the dominant hadroproduction cross section in proton-proton collisions. Following the stringent bounds on generic SUSY models obtained with $\sqrt{s} = 7$ TeV data, ATLAS and CMS moved the focus of their SUSY searches to the so-called *natural* SUSY models [1]. In its minimal realization, a natural SUSY spectrum is composed of the minimum set of SUSY partners needed to protect the mass of the Higgs (H) boson from quantum corrections: a gluino, one bottom squark, two top squarks, and three higgsinos (two neutral and one charged). This SUSY scenario results in events with multiple top and bottom quarks, produced in association with missing transverse energy E_T^{miss} . No evidence for the production of such particles has been found, pushing the allowed mass range for gluinos and top squarks above ~ 1600 GeV and ~ 700 GeV, respectively, for a low-mass neutralino LSP and largely independent of the top squark and gluino branching ratios (see for instance Ref. [2, 3]).

In a few cases, a data yield above the expected background was observed for certain signal regions, for example, in the case of the *edge* dilepton analysis by CMS [4] and the SUSY search in Z+jets events by ATLAS [5]. These excesses correspond to, respectively, $\sim 2.4\sigma$ and $\sim 3.0\sigma$ of local significance, which are reduced after accounting for the look-elsewhere effect (LEE). Several interpretations of these results were given in the literature [6–11], mainly related to the electroweak production

of SUSY particles with long decay chains.

Here we discuss the re-interpretation of the search for electroweak SUSY partners in $H(\gamma\gamma) + \geq 1$ jet events by the CMS collaboration performed at 8 TeV [12]. The analysis uses the diphoton invariant mass $m_{\gamma\gamma}$ to select events with a H-like candidate. The non-resonant (mostly QCD diphoton production) and resonant (standard model $H(\gamma\gamma)$ production) backgrounds are estimated using the $m_{\gamma\gamma}$ sidebands in data and the Monte Carlo simulation, respectively. The background prediction is performed as a function of the razor variables M_R and R^2 in five mutually exclusive *boxes*, targeting different final states: high- p_T $H(\gamma\gamma)$ (**HighPt** box), $H(\gamma\gamma) + H(b\bar{b})$ (**Hbb** box), $H(\gamma\gamma) + Z(b\bar{b})$ (**Zbb** box), and low- p_T $H(\gamma\gamma)$ with high- and low-resolution photons (**HighRes** and **LowRes** boxes, respectively). Five events are observed in one (M_R, R^2) bin of the **HighRes** box, compared to less than one expected background event. This corresponds to a local significance of 2.9σ , reduced to 1.6σ after the LEE.

In this paper, we propose and study a new interpretation of this search in terms of SUSY models with light quarks. We emulate this CMS analysis to derive bounds on squark production. Since the analysis does not require or veto jets originating from b-quarks (b-jets), the results apply to bottom-squark production in natural SUSY models.

Recently, an updated search was performed with data collected at 13 TeV [13]. One of the models proposed during the studies presented in this paper (model B) was also used for the interpretation of the results.

BENCHMARK SIGNAL MODELS

We consider two simplified models with bottom squark pair production, both resulting in a H+jets final state.

In the first model, hereafter referred to as **model A**, we consider the asymmetric production of a $\tilde{b}_2\tilde{b}_1$ pair, where \tilde{b}_2 and \tilde{b}_1 are the heaviest and the lightest bottom squarks, respectively. The \tilde{b}_2 decays to $b\tilde{\chi}_2^0$, with $\tilde{\chi}_2^0 \rightarrow H\tilde{\chi}_1^0$. The lightest neutralino $\tilde{\chi}_1^0$ is assumed to be

*jduarte@caltech.edu; now at Fermi National Accelerator Laboratory.

†Now at Harvard University.

the LSP. The \tilde{b}_1 , close in mass to the LSP, decays to $b\tilde{\chi}_1^0$. All the other SUSY partners are assumed to be too heavy to be produced at the LHC and are ignored in this analysis. This model represents a new mechanism for the production of $H + 2b$ -jets + invisible, with one of the associated b -jets typically having low momentum.

In the second model, hereafter referred to as model B [14], two bottom squarks $\tilde{b}_1\tilde{b}_1$ are produced, each decaying as $\tilde{b}_1 \rightarrow b\tilde{\chi}_2^0$. The $\tilde{\chi}_2^0$ then decays to $H\tilde{\chi}_1^0$, the $\tilde{\chi}_1^0$ being the LSP. As for model A, the other SUSY partners are ignored. This simplified model corresponds to a final state consisting of $2H + 2b$ -jets + invisible.

The mass spectrum for each model is shown in Fig. 1. We fix the $\tilde{\chi}_2^0$ and $\tilde{\chi}_1^0$ masses to 230 GeV and 100 GeV, respectively. In model A, we fix the \tilde{b}_1 mass to 130 GeV as varying its mass in between the limits of the $\tilde{\chi}_1^0$ and $\tilde{\chi}_2^0$ masses has little effect. Finally, we scan the \tilde{b}_2 (\tilde{b}_1) mass between 250 GeV and 800 GeV for model A (B). These assumptions do not limit the conclusions derived on the squark production cross section. In fact, the analysis is sensitive to mass differences and not to the absolute mass of SUSY partners. On the other hand, the chosen LSP and NLSP masses does play a role when the cross section limits are translated in terms of mass exclusion bounds.

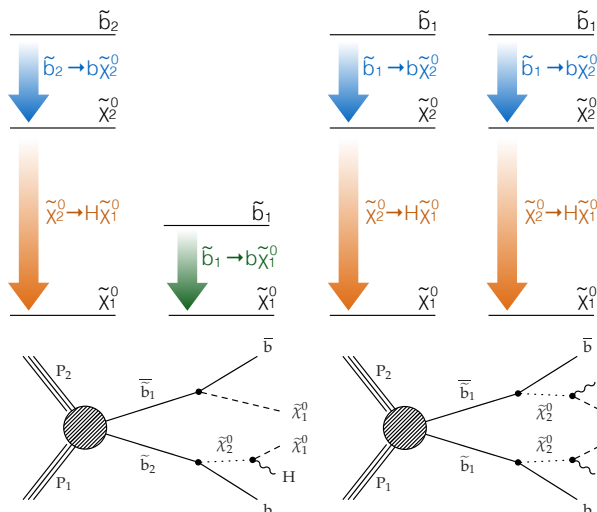


FIG. 1: Pictorial representation of the decay chains and event topologies associated with model A (left) and model B (right), as described in the text.

EVENT GENERATION AND DETECTOR SIMULATION

The study is performed using samples of Monte Carlo events. The event generation is performed in PYTHIA 8.210 [15, 16]. The default parton density function set is NNPDF 2.3 QCD+QED LO (with

TABLE I: Photon isolation requirements, as in Ref [23].

The photon isolation variables, I_γ , I_n , and I_π , are computed by summing the transverse momenta of photons, neutral hadrons, and charged hadrons, respectively, inside an isolation cone of radius $\Delta R = 0.3$ around the selected photon.

I_γ	barrel	$1.3 \text{ GeV} + 0.005p_T^\gamma$
	endcap	–
I_n	barrel	$3.5 \text{ GeV} + 0.04p_T^\gamma$
	endcap	$2.9 \text{ GeV} + 0.04p_T^\gamma$
I_π	barrel	2.6 GeV
	endcap	2.3 GeV

$\alpha_s(m_Z) = 0.130$) [17–19]. Fast simulation of the detector is performed in DELPHES 3.3.2 [20]. The default description of CMS as provided in the release is used, except for a modification to the photon isolation and efficiency, described in the next section. Jet clustering is performed using FASTJET 3.1.3 [21]. As in CMS, the anti- k_T jet clustering algorithm is used with jet-size parameter $R = 0.5$ [22].

EMULATION OF THE CMS SEARCH

The emulated event selection is summarized as follows,

- Events with two isolated photons with $p_T > 25$ GeV and $|\eta| < 1.44$ are selected. As in Ref. [23], the photon isolation variables, I_γ , I_n , and I_π , are computed by summing the transverse momenta of photons, neutral hadrons, and charged hadrons, respectively, inside an isolation cone of radius $\Delta R = 0.3$ around the selected photon. The photon isolation requirements on these variables are shown in Tab I. An additional photon selection efficiency is applied in DELPHES such that isolated photons with $p_T < 10$ GeV ($p_T \geq 10$ GeV) are randomly selected with 94% (98%) efficiency.
- Events with one H candidate with $p_T > 20$ GeV are selected. A pair of selected photons is considered an H candidate if at least one photon has $p_T > 40$ GeV and the diphoton mass $m_{\gamma\gamma} > 100$ GeV. If the event contains more than one H candidate, the one with the highest scalar sum p_T of the two photons is selected.
- Jets are reconstructed using the FASTJET [21] implementation of the anti- k_T [22] algorithm with jet radius parameter $R = 0.5$.
- Events with at least one jet with $p_T > 30$ GeV and $|\eta| < 3.0$ are selected.
- An emulation of the “medium” requirement (mistag probability of 1% and b-tag efficiency of

$\sim 68\%$) of the combined secondary vertex (CSV) b-tagging algorithm is used to identify b-jets [24].

- A $b\bar{b}$ candidate pair is identified if both jets satisfy the medium requirement of the b-tagging algorithm (note: the CMS analysis requires only one to satisfy the medium requirement, while both are required to satisfy the loose requirement).
- The $b\bar{b}$ candidate pair with the mass closest to 125 GeV or 91.2 GeV is chosen as the $H \rightarrow b\bar{b}$ or $Z \rightarrow b\bar{b}$ candidate, respectively.
- The razor variable M_R , calculated from two megajets [25] is required to be greater than 150 GeV. All possible combinations of the reconstructed jets and the $H(\gamma\gamma)$ candidate are clustered to form megajets. The pair of megajets that minimizes the sum in quadrature of the invariant masses of the two megajets is selected.

After this baseline selection, events are categorized according to the following requirements,

- **HighPt**: all events with an $H \rightarrow \gamma\gamma$ candidate with $p_T > 110$ GeV.
- **Hbb**: remaining events with a $H \rightarrow b\bar{b}$ candidate with mass $110 \geq m_{b\bar{b}} \geq 140$ GeV.
- **Zbb**: remaining events with a $Z \rightarrow b\bar{b}$ candidate with mass $76 \geq m_{b\bar{b}} \geq 106$ GeV.
- **HighRes**: 70% of remaining events after the **Zbb** selection (emulating the efficiency of the “high-resolution photon” selection).
- **LowRes**: all remaining events.

We assume the breakdown of events between the **HighRes** box and **LowRes** box is 70%-to-30% after the **Zbb** selection. This is based on the following observations: (i) CMS categorizes events in the **HighRes** box if both photons in the event satisfy $\sigma_E/E < 0.015$, where σ_E/E is the estimated relative energy resolution, and categorizes events in the **LowRes** box otherwise, (ii) CMS observes a similar 70%-to-30% breakdown for both SM Higgs production and electroweak SUSY processes in Monte Carlo simulation [12], and (iii) we expect this breakdown to be model-independent assuming both photons are real and come from the decay of a Higgs boson, as it is based on the properties of such photons detected in CMS and not on the details of the model.

Finally, the search region selection is as follows,

- The search region in the $m_{\gamma\gamma}$ distribution is defined by $(125 - 2\sigma_{\text{eff}}, 126 + 2\sigma_{\text{eff}})$ in each event category, where σ_{eff} is defined such that $\sim 68\%$ of Higgs boson events fall in an interval of $\pm\sigma_{\text{eff}}$ around the

nominal m_H value. Following this procedure using our generated and simulated signal samples, we derive σ_{eff} to be 3.8 GeV in the **HighPt** box and 2.2 GeV in the **HighRes** and **LowRes** boxes. For the **Hbb** and **Zbb** boxes, due to the low number of selected signal events, we use the overall average value of 2.8 GeV.

We note that these σ_{eff} values are larger than the corresponding ones in Ref. [12]. This is due to the larger width observed for the diphoton mass distribution in Higgs boson events simulated and reconstructed with DELPHES, compared to official CMS software. This implies the effective diphoton mass resolution when using DELPHES is larger than in the real CMS detector. We attempt to account for this with a modification explained in Sec. .

BAYESIAN STATISTICAL INTERPRETATION

We model the likelihood according to a Poisson density, considering the expected background yield (with associated uncertainty), the expected signal yield (for a given signal cross section), and the observed yield. The background uncertainty is modeled with a gamma density. The background yields and the corresponding uncertainties are taken from the tables provided in Ref. [12]. To take into account systematic uncertainties on the signal, we assign a 30% uncertainty (assuming a log-normal density) on the signal strength, a multiplicative factor modifying the signal cross section. We then derive the posterior density for the signal cross section σ as:

$$p(\sigma|\text{data}) \propto \mathcal{L}(\text{data}|\sigma)p_0(\sigma), \quad (1)$$

where $\mathcal{L}(\text{data}|\sigma)$ is the likelihood and $p_0(\sigma)$ is the prior density taken to be uniform. The likelihood is then

$$\begin{aligned} \mathcal{L}(\text{data}|\sigma) &= \int_0^\infty d\mu \text{Ln}(\mu|\bar{\mu}, \delta\mu) \\ &\times \prod_{i=0}^{n_{\text{bins}}} \int_0^\infty db_i \text{Poisson}(n_i|L\mu\sigma\epsilon_i + b_i) \\ &\times \Gamma(b_i|\bar{b}_i, \delta b_i), \end{aligned} \quad (2)$$

where the product runs over the number of bins n_{bins} ; n_i is the observed yield in the i^{th} bin, L is the integrated luminosity, b_i is the assumed value of the background yield in the i^{th} bin and $\bar{b}_i \pm \delta b_i$ is its expected value and the associated uncertainty; ϵ_i is the nominal value of the signal efficiency times acceptance in the i^{th} bin; μ is the signal strength, a nuisance parameter modifying the signal cross section (nominally equal to $\bar{\mu} = 1$ with a $\delta\mu = 30\%$ uncertainty); $\text{Ln}(x|m, \delta)$ is the log-normal distribution for x , parameterized such that $\log(m)$ is the mean and $\log(1+m\delta)$ is the standard deviation of the log of the distribution; $\Gamma(x|m, \delta)$ is the gamma distribution

for x , parameterized such that m is the mode and δ^2 is the variance of the distribution. The 95% credibility level (CL) upper limit on the signal cross section σ_{up} is obtained from the posterior, such that

$$\frac{\int_0^{\sigma_{\text{up}}} d\sigma p(\sigma|\text{data})}{\int_0^{\infty} d\sigma p(\sigma|\text{data})} = 0.95 . \quad (4)$$

We also utilize a signal significance measure defined by

$$Z(\sigma) = \text{sign}[\log B_{10}(\text{data}, \sigma)] \sqrt{2|\log B_{10}(\text{data}, \sigma)|} , \quad (5)$$

where

$$B_{10}(\text{data}, \sigma) = \frac{\mathcal{L}(\text{data}|\sigma, H_1)}{\mathcal{L}(\text{data}|H_0)} \quad (6)$$

is the *local* Bayes factor for the data for a given signal cross section σ , and $\mathcal{L}(\text{data}|\sigma, H_1)$ and $\mathcal{L}(\text{data}|H_0)$ are the likelihoods for the signal-plus-background (H_1) and background-only (H_0) hypotheses, respectively. As described in Ref. [26], this measured is a signed Bayesian analog of the frequentist “n-sigma.” For each signal model with specified masses, we scan the signal cross section σ to find the maximum significance, which occurs at the mode of the posterior.

CORRECTION AND VALIDATION

As discussed above, we find differences in the performance of the emulated CMS detector and the real CMS detector, e.g. the larger diphoton mass resolution. To take into account this and other differences in the detector simulation and reconstruction performed by DELPHES and official CMS software, we conservatively double the background uncertainties in each bin reported by CMS in Ref. [12] when evaluating the likelihood in Eqn. 3. We find this conservative approach better reproduces the observed and expected limits on a benchmark simplified model.

To validate our emulation result, we produced 95% CL limits on the production cross section of an electroweak simplified model of $\tilde{\chi}_1^\pm \tilde{\chi}_2^0$ production, followed by the decays $\tilde{\chi}_1^\pm \rightarrow W^\pm \tilde{\chi}_1^0$, $\tilde{\chi}_2^0 \rightarrow H \tilde{\chi}_1^0$. For this model, CMS provided the 95% confidence level upper limits on the cross section assuming an LSP mass of $m_{\tilde{\chi}_1^0} = 1$ GeV and equal chargino and second neutralino masses, $m_{\tilde{\chi}_1^\pm} = m_{\tilde{\chi}_2^0}$.

The comparison between our result and the CMS result for this model is shown in figure 2 as a function of $m_{\tilde{\chi}_1^\pm}$.

RESULTS

Figures 3-5 contain the results of the reinterpretation of the CMS data for both models. To show how well signal model A agrees with the excess observed by CMS,

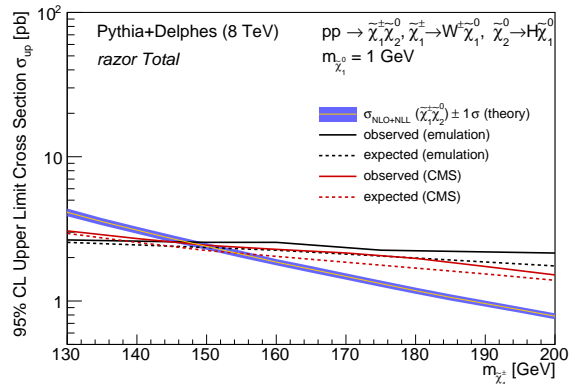


FIG. 2: Comparison between the CMS result (red) and our emulation (black). Note, this scan assumes $m_{\tilde{\chi}_1^0} = 1$ GeV and $m_{\tilde{\chi}_1^\pm} = m_{\tilde{\chi}_2^0}$.

Fig. 3 (top) displays the expected SM background distribution and uncertainty taken from the CMS result compared to the distribution of the signal events for $m_{\tilde{b}_2}^- = 500$ GeV and $m_{\tilde{b}_2}^- = 800$ GeV, with other mass parameters set as $m_{\tilde{b}_2}^- = 130$ GeV, $m_{\tilde{\chi}_2^0} = 230$ GeV, and $m_{\tilde{\chi}_1^0} = 100$ GeV. The bin numbers correspond to the order of the signal regions in the yield tables in Ref. [12] and are reproduced in Tab. II. The normalization for each sig-

TABLE II: HighRes bin numbering scheme as in Ref. [12].

Bin	M_R range	R^2 range
0	[150, 250]	[0.00, 0.05]
1	[150, 250]	[0.05, 0.10]
2	[150, 250]	[0.10, 0.15]
3	[150, 250]	[0.15, 1.00]
4	[250, 400]	[0.00, 0.05]
5	[250, 400]	[0.05, 0.10]
6	[250, 400]	[0.10, 1.00]
7	[400, 1400]	[0.00, 0.05]
8	[400, 1400]	[0.05, 1.00]
9	[1400, 3000]	[0.00, 1.00]

nal model is taken from the mode (i.e. “best-fit”) signal cross section of the posterior density in the HighRes box. Fig. 4 (top), shows the 95% CL combined upper limit on the cross section for model A. Finally, Fig. 5 (top) shows the maximum significance Z as well as the best fit signal cross section for model A as a function of $m_{\tilde{b}_2}^-$.

The bottom of Fig. 3-5 are the analogous results for model B. The chosen model B mass points in Fig. 3 are $m_{\tilde{b}_1}^- = 500$ GeV or $m_{\tilde{b}_1}^- = 800$ GeV, $m_{\tilde{\chi}_2^0} = 230$ GeV, and $m_{\tilde{\chi}_1^0} = 100$ GeV. The limit and significance scans in Fig. 4 and 5 are performed as a function of the \tilde{b}_1 mass. For model B, we also compare both the excluded cross section at 95% CL and the best-fit cross section as a function of the \tilde{b}_1 mass to the NLO+NLL pre-

dicted cross section at $\sqrt{s} = 8$ TeV [27–32]. We find the 8 TeV data excludes bottom squark pair production below $m_{\tilde{b}_1} = 330$ GeV for the chosen neutralino masses of $m_{\tilde{\chi}_2^0} = 230$ GeV and $m_{\tilde{\chi}_1^0} = 100$ GeV. More interestingly, the largest combined significance is 1.8σ for $m_{\tilde{b}_1} = 500$ GeV and the best-fit cross section is 0.4 pb, which is of the same order of magnitude as the predicted cross section.

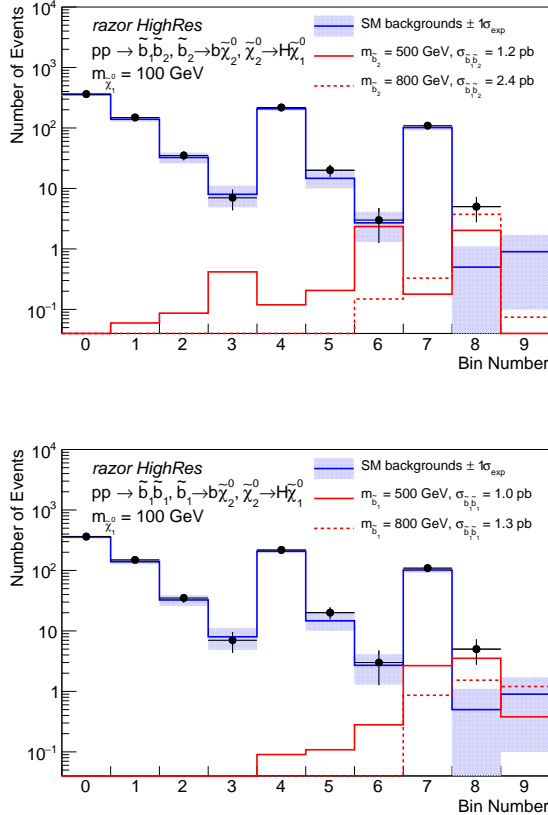


FIG. 3: (Top) The expected background and uncertainty (multiplied by a factor of two as explained in the text) compared to the best-fit signal distribution in the **HighRes** box for two particular mass points, $m_{\tilde{b}_2} = 500$ GeV and $m_{\tilde{b}_2} = 800$ GeV, in model A. (Bottom) The expected background and uncertainty (multiplied by a factor of two as explained in the text) compared to the best-fit signal distribution in the **HighRes** box for two particular mass points, $m_{\tilde{b}_1} = 500$ GeV and $m_{\tilde{b}_1} = 800$ GeV, in model B. The bin numbers correspond to the order of the signal regions in the yield tables in Ref. [12] and are reproduced in Tab. II.

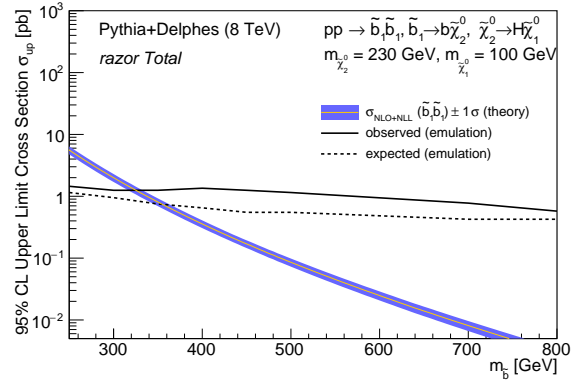
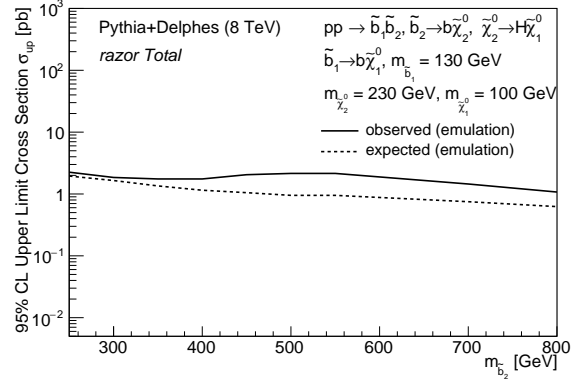


FIG. 4: (Top) The 95% CL upper limit on the cross section on $\tilde{b}_1\tilde{b}_2$ production in model A as a function of $m_{\tilde{b}_2}$ (black). (Bottom) The 95% CL upper limit on the cross section on $\tilde{b}_1\tilde{b}_1$ production in model B as a function of $m_{\tilde{b}_1}$ (black) compared to the NLO+NLL predicted cross section (yellow). Note, these scans assume $m_{\tilde{\chi}_1^0} = 100$ GeV, $m_{\tilde{\chi}_2^0} = 230$ GeV, and for model A $m_{\tilde{b}_1} = 130$ GeV.

DISCUSSION AND SUMMARY

In this paper, we proposed two simplified models of bottom squark pair production for use in the interpretation of an excess observed by CMS in a search for SUSY in H+jets events using razor variables at $\sqrt{s} = 8$ TeV [12]. In model A, we considered the asymmetric production of a $\tilde{b}_2\tilde{b}_1$ pair, with the $\tilde{b}_1 \rightarrow \tilde{\chi}_1^0$, $\tilde{b}_2 \rightarrow b\tilde{\chi}_2^0$, and $\tilde{\chi}_2^0 \rightarrow H\tilde{\chi}_1^0$, where $\tilde{\chi}_1^0$ is a neutralino LSP and we fix the mass splitting $m_{\tilde{\chi}_2^0} - m_{\tilde{\chi}_1^0} = 130$ GeV. In model B, we considered the symmetric production of a $\tilde{b}_1\tilde{b}_1$ pair, with $\tilde{b}_1 \rightarrow b\tilde{\chi}_2^0$, $\tilde{\chi}_2^0 \rightarrow H\tilde{\chi}_1^0$, and $m_{\tilde{\chi}_2^0} - m_{\tilde{\chi}_1^0} = 130$ GeV.

We scanned the bottom squark masses for a fixed LSP mass of $m_{\tilde{\chi}_1^0} = 100$ GeV for both models and quantified the agreement with the data. We found the excess observed in data is broadly consistent with both models, with the largest signal significance being 1.8σ correspond-

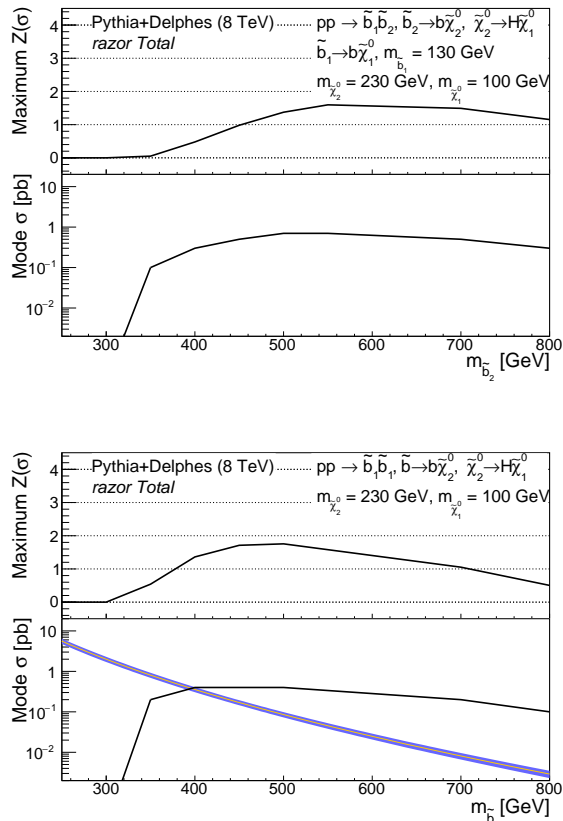


FIG. 5: (Top) The maximum significance $Z(\sigma)$ for a given $m_{\tilde{b}_2}$ in the top panel and the “best fit” signal cross section σ in the bottom panel for model A. (Bottom) The maximum significance $Z(\sigma)$ for a given $m_{\tilde{b}_1}$ in the top panel and the “best fit” signal cross section σ in the bottom panel for model B. Note, these scans assume $m_{\tilde{\chi}_1^0} = 100$ GeV, $m_{\tilde{\chi}_2^0} = 230$ GeV, and for model A $m_{\tilde{b}_1} = 130$ GeV.

ing to model B with $m_{\tilde{b}_1} = 500$ GeV, $m_{\tilde{\chi}_2^0} = 230$ GeV, and $m_{\tilde{\chi}_1^0} = 100$ GeV. Following this study, model B used by the CMS collaboration to interpret the results of the updated 13 TeV search for SUSY in the same channel [13], which also exhibits an excess possibly consistent with the model.

ACKNOWLEDGEMENTS

This work is funded by the California Institute of Technology High Energy Physics under Contract DE-SC0011925 with the United States Department of Energy. The authors are grateful to the international collaborations of scientists whose work resulted in the discovery of the Higgs boson at the LHC in 2012 and especially the SUSY searches group of the CMS collaboration. The work is motivated by results obtained as part of the

- [1] Michele Papucci, Joshua T. Ruderman, and Andreas Weiler. Natural SUSY Endures. *JHEP*, 09:035, 2012.
- [2] Vardan Khachatryan et al. Search for Supersymmetry Using Razor Variables in Events with b -Tagged Jets in pp Collisions at $\sqrt{s} = 8$ TeV. *Phys. Rev.*, D91:052018, 2015.
- [3] Inclusive search for supersymmetry using the razor variables at $\sqrt{s} = 13$ TeV. Technical Report CMS-PAS-SUS-15-004, CERN, Geneva, 2015.
- [4] Search for physics beyond the standard model in events with two opposite-sign same-flavor leptons, jets, and missing transverse energy in pp collisions at $\sqrt{s} = 8$ TeV. Technical Report CMS-PAS-SUS-12-019, CERN, Geneva, 2014.
- [5] Georges Aad et al. Search for supersymmetry in events containing a same-flavour opposite-sign dilepton pair, jets, and large missing transverse momentum in $\sqrt{s} = 8$ TeV pp collisions with the ATLAS detector. *Eur. Phys. J.*, C75(7):318, 2015. [Erratum: *Eur. Phys. J.* C75,no.10,463(2015)].
- [6] Peisi Huang and Carlos E. M. Wagner. CMS kinematic edge from sbottoms. *Phys. Rev.*, D91(1):015014, 2015.
- [7] Ben Allanach, Are R. Raklev, and Anders Kvellestad. Interpreting a CMS excess in $lljj + \text{missing}$ -transverse-momentum with the golden cascade of the minimal supersymmetric standard model. *Phys. Rev.*, D91(11):115022, 2015.
- [8] Ben Allanach, Are Raklev, and Anders Kvellestad. Consistency of the recent ATLAS $Z + E_T^{\text{miss}}$ excess in a simplified GGM model. *Phys. Rev.*, D91:095016, 2015.
- [9] Junjie Cao, Liangliang Shang, Jin Min Yang, and Yang Zhang. Explanation of the ATLAS Z-Peaked Excess in the NMSSM. *JHEP*, 06:152, 2015.
- [10] Ulrich Ellwanger. Possible explanation of excess events in the search for jets, missing transverse momentum and a Z boson in pp collisions. *Eur. Phys. J.*, C75(8):367, 2015.
- [11] Archil Kobakhidze, Ning Liu, Lei Wu, and Jin Min Yang. ATLAS Z-peaked excess in the MSSM with a light sbottom or stop. *Phys. Rev.*, D92(7):075008, 2015.
- [12] Search for SUSY with Higgs in the diphoton final state using the razor variables. Technical Report CMS-PAS-SUS-14-017, CERN, Geneva, 2015.
- [13] Search for SUSY in Events with a Higgs Decaying to Two Photons Using the Razor Variables. Technical Report CMS-PAS-SUS-16-012, CERN, Geneva, 2016.
- [14] Ann Miao Wang. New Physics Models in the Diphoton Final State at CMS, 2015. DOI 10.7907/Z9CC0XMN. <http://resolver.caltech.edu/CaltechTHESIS:01152016-102117113>.
- [15] Torbjorn Sjostrand, Stephen Mrenna, and Peter Z. Skands. PYTHIA 6.4 Physics and Manual. *JHEP*, 05:026, 2006.
- [16] Torbjörn Sjöstrand, Stefan Ask, Jesper R. Christiansen, Richard Corke, Nishita Desai, Philip Ilten, Stephen Mrenna, Stefan Prestel, Christine O. Rasmussen, and Peter Z. Skands. An Introduction to PYTHIA 8.2. *Comput. Phys. Commun.*, 191:159–177, 2015.

- [17] Richard D. Ball, Valerio Bertone, Stefano Carrazza, Luigi Del Debbio, Stefano Forte, Alberto Guffanti, Nathan P. Hartland, and Juan Rojo. Parton distributions with QED corrections. *Nucl. Phys.*, B877:290–320, 2013.
- [18] Stefano Carrazza. Towards the determination of the photon parton distribution function constrained by LHC data. *PoS, DIS2013:279*, 2013.
- [19] Stefano Carrazza. Towards an unbiased determination of parton distributions with QED corrections. In *Proceedings, 48th Rencontres de Moriond on QCD and High Energy Interactions*, pages 357–360, 2013.
- [20] J. de Favereau, C. Delaere, P. Demin, A. Giammanco, V. Lemaitre, A. Mertens, and M. Selvaggi. DELPHES 3, A modular framework for fast simulation of a generic collider experiment. *JHEP*, 02:057, 2014.
- [21] Matteo Cacciari, Gavin P. Salam, and Gregory Soyez. FastJet User Manual. *Eur. Phys. J.*, C72:1896, 2012.
- [22] Matteo Cacciari, Gavin P. Salam, and Gregory Soyez. The Anti-k(t) jet clustering algorithm. *JHEP*, 04:063, 2008.
- [23] Vardan Khachatryan et al. Performance of Photon Reconstruction and Identification with the CMS Detector in Proton-Proton Collisions at $\sqrt{s} = 8$ TeV. *JINST*, 10(08):P08010, 2015.
- [24] Serguei Chatrchyan et al. Identification of b-quark jets with the CMS experiment. *JINST*, 8:P04013, 2013.
- [25] Serguei Chatrchyan et al. Search for supersymmetry with razor variables in pp collisions at $\sqrt{s} = 7$ TeV. *Phys. Rev. D*, 90(11):112001, 2014.
- [26] Phenomenological MSSM interpretation of CMS results at $\sqrt{s} = 7$ and 8 TeV. Technical Report CMS-PAS-SUS-15-010, CERN, Geneva, 2015.
- [27] W. Beenakker, R. Höpker, M. Spira, and P. M. Zerwas. Squark and gluino production at hadron colliders. *Nucl. Phys. B*, 492:51, 1997.
- [28] A. Kulesza and L. Motyka. Threshold resummation for squark-antisquark and gluino-pair production at the LHC. *Phys. Rev. Lett.*, 102:111802, 2009.
- [29] A. Kulesza and L. Motyka. Soft gluon resummation for the production of gluino-gluino and squark-antisquark pairs at the LHC. *Phys. Rev. D*, 80:095004, 2009.
- [30] W. Beenakker, S. Brensing, M. Krämer, A. Kulesza, E. Laenen, and I. Niessen. Soft-gluon resummation for squark and gluino hadroproduction. *JHEP*, 12:041, 2009.
- [31] W. Beenakker, S. Brensing, M. Krämer, A. Kulesza, E. Laenen, L. Motyka, and I. Niessen. Squark and gluino hadroproduction. *Int. J. Mod. Phys. A*, 26:2637, 2011.
- [32] Christoph Borschensky, Michael Krmer, Anna Kulesza, Michelangelo Mangano, Sanjay Padhi, Tilman Plehn, and Xavier Portell. Squark and gluino production cross sections in pp collisions at $\sqrt{s} = 13, 14, 33$ and 100 TeV. *Eur. Phys. J.*, C74(12):3174, 2014.
- [33] Alex Mott. Search for Higgs Boson Production Beyond the Standard Model Using the Razor Kinematic Variables in pp Collisions at $\sqrt{s}=8$ TeV, 2015. doi:10.7907/Z9XK8CHR. <http://resolver.caltech.edu/CaltechTHESIS:05052015-155442785>.